JMEPEG (2018) 27:447–456
https://doi.org/10.1007/s11665-018-3127-y

1059-9495/$19.00

# Surface Condition of New γ–γ′ Co-Al-Mo-Nb and Co-Al-W Cobalt-Based Superalloys After Oxidation at 800 °C

*Damian Migas, Grzegorz Moskal, and Dawid Niemiec*

*(Submitted June 7, 2017; in revised form November 8, 2017; published online January 19, 2018)*

**A new type γ–γ′ Co-Al-Mo-Nb Co-based superalloys were developed due to limitations of basic Co-Al-W superalloys, related to tungsten alloying. The present study aims to characterization of new γ–γ′ Co-10Al-5Mo-2Nb (at.%) cobalt-based superalloy performance in terms of the high-temperature exposure under cyclic conditions, with particular regard to surface condition. Specimens were tested in cycles of high-temperature exposition (25, 50, 75, 100 and 150 h) in air environment at 800 °C. Detailed analysis of oxidized surfaces by scanning electron microscopy, energy-dispersive spectroscopy and x-ray diffraction was made at various intervals during testing. The cyclic oxidation behavior of new alloy was compared to the basic Co-9Al-9W (at.%) Co-based superalloy.**

**Keywords** γ–γ′ cobalt-based superalloys, Co-Al-Mo-Nb superalloy, Co-Al-W superalloy, cyclic oxidation, surface condition

## 1. Introduction

The ever-increasing needs for high efficiency in high-temperature applications, i.e., gas turbines for power plants and aircraft engines, require development of heat-resistant materials. Ni-based superalloys exhibit more appropriate combination of creep properties and damage tolerance in comparison with that of Fe-based intermetallics and conventional Co-based superalloys owing to γ′-$L1_2$ phase strengthening mechanism. For improvement of the creep resistance, these alloys are solidified into single crystals and thereby may be utilized in the highest-temperature applications (Ref 1, 2). Although Ni-based superalloys are used commonly, the inlet temperature in turbine is approaching the melting point of most of advanced single-crystal superalloys. Furthermore, the substantial limitation of these alloys is insufficient resistance to hot corrosion and sulfide corrosion that involves utilization of special bond coatings, which are expensive, technologically challenging and still insufficient in terms of long exposure at high temperature (Ref 3). Taking into account the limitations of Ni-based superalloys, the development of new generations of superalloys is necessary nowadays. Although the conventional Co-based superalloys possess inferior creep strength to nickel alloys with the γ–γ′ microstructure, their resistance to oxidation and corrosion in sulfur-rich high-temperature environments is remarkable (Ref 4-7). The most appropriate solution would be combination of Ni-based and Co-based superalloys' properties, providing appropriate creep resistance and resistance to oxidation and corrosion as well.

**Damian Migas, Grzegorz Moskal** and **Dawid Niemiec,** Institute of Materials Engineering, Silesian University of Technology, Krasinskiego 8 Str, 40-019 Katowice, Poland. Contact e-mail: damian.migas@outlook.com.

This challenge has been taken in 2006 by Sato et al. (Ref 8). The γ′-$Co_3$(Al, W) phase with an $L1_2$ structure, analogous to γ′-$Ni_3Al$ was discovered in the Co-Al-W ternary system. The formation of the coherent two-phase microstructure, where submicron γ′-$Co_3$(Al, W) cuboidal precipitates align regularly within the γ-Co matrix, is available due to small lattice misfit between the *fcc* γ-Co matrix and γ′ phase. These alloys based on Co-Al-W system are characterized by higher melting points than those of analogous Ni-based superalloys with morphologically similar microstructure and hence have gained considerable interest due to their potential as a new generation of superalloys (Ref 9-11).

Besides the creep resistance and corrosion properties, the high-temperature oxidation resistance is essential issue that should be considered before implementation of the new class of superalloys. Few studies have been carried out in order to examine the oxidation performance of new Co-Al-W Co-based alloys (Ref 12-16). Their oxidation at 800 °C results in the formation of a three-layered scale. The external layer has been recognized as $Co_3O_4$. The layer underneath contains mixed oxides composed of Al, W and other alloying elements, although inner layer is suggested to be $Al_2O_3$ layer. The substrate alloy beneath the growing oxide is depleted in Al; hence, the γ′ fraction decreases, while high-aspect-ratio $Co_3W$ precipitates are formed (Ref 17). It has been found that Co-oxides do not provide acceptable protection for substrate alloy and are prone to spallation during cooling (Ref 13, 18, 19); therefore, it is important to understand the oxidation performance and how it might be modified through alloying. Generally, it was noted that Cr and Si additions help form protective layers of chromia and silica, resulting in the improvement of oxidation resistance (Ref 20). Furthermore, the positive influence of Cr and Si on the oxidation resistance of novel γ–γ′ Co-based superalloys was proved (Ref 19); however, the excessive additions of Cr destabilize the γ/γ′ microstructure. The effect of alloying elements on the oxidation behavior of Co-Al-W Co-based superalloys under conditions of cyclic exposure to high temperature was analyzed as well (Ref 17, 19). However, the considerable disadvantage of this group of alloys is connected with introduction of W, which clearly affects increase in density to approximately 9.5 g/$cm^3$.

Furthermore, the homogenization of these alloys is challenging due to W-content. The another essential limitation is fact that W reacts with Co and forms deleterious phase $Co_3W$ with $D0_{19}$ structure (Ref 21).

The possibility of W-replacement was analyzed in several studies (Ref 22-24). Mo is element promoting γ′ formation and hence may replace tungsten in Co-based superalloys. In 2015 occurred the first data concerning new W-free γ–γ′ Co-Al-Mo-Nb Co-based superalloys (Ref 3, 25, 26). The density of Nb-containing superalloys was 8.25-8.355 g $cm^{-3}$, therefore definitely lower compared to that of Co-7W-7Al alloy (at.%), characterized by density equal 9.2 g $cm^{-3}$. Furthermore, the specific strength of new Co-based superalloys was considerably higher—respectively, 96 and 79 MPa $g^{-1}$ $cm^{-3}$. The thermogravimetric investigations of Co-Al-Mo-Nb with Ni-addition have been performed (Ref 27). Although the papers concerning Co-Al-Mo-Nb Co-based superalloys are available, the amount of data regarding this new group of alloys is still insufficient, particularly regarding the oxidation and corrosion resistance.

In the present paper, characterization of high-temperature cyclic oxidation of Co-10Al-5Mo-2Nb (at.%) as-cast alloy was performed. The specimen made of γ-γ′ Co-based alloy was exposed to long-term cyclic oxidation at 800 °C, which is related to real conditions in turbine engines. The oxidation performance of alloy under these conditions was determined, inclusive of mass change observations and analysis of the grown scale. Moreover, the obtained cyclic oxidation characteristics were compared to basic Co-9Al-9W (at.%) alloy.

## 2. Experimental Methods

The as-cast Co-10Al-5Mo-2Nb and Co-9Al-9W (at.%) alloys are subject of the present research. The investigated alloys were melted using induction vacuum furnace VSG 02 Balzers and casted into cold graphite molds under argon atmosphere. The final products of casting process were rods of size ø20 × 100 mm (Fig. 1). The measured compositions of obtained casts are present in Table 1. The microstructures of investigated alloys were typical as-cast dendritic microstructures characteristic for ingots solidifying under conditions of fast and directional heat dissipation. In case of Co-9Al-9W (at.%), the high chemical homogeneity was obtained (Ref 28); however, within microstructure of Co-10Al-5Mo-2Nb (at.%) alloy, tiny precipitates rich in Mo and Nb were observed and recognized (Co3Mo and Co3Nb) via x-ray diffraction.

Afterward, the specimens ø20 × 5 mm were cut from the casted rods, and the surfaces were ground, cleaned and degreased. The cylindrical specimens were placed in flat bottomed alumina crucibles and tested in laboratory furnace atmosphere at 800 °C. In order to contain spalled oxidation products, lids were placed on the crucibles before weight measurements during periodic removal of specimens and cooling in open air. Each cycle of oxidation was performed according to the following proceeding: (1) placement of the samples into the laboratory furnace at temperature 800 °C; (2) exposure of specimen in the furnace for allotted extent of time (25 h); (3) removal of the specimens from the furnace at 800 °C; (4) cooling of the specimens out of the furnace to room temperature; (5) specimen mass measurements using laboratory balance with a resolution of 0:10 mg; and (6) determination of the surface condition, i.e., analysis of morphology, phase and chemical composition of the grown scale.

**Fig. 1** Macrograph of Co-based alloy cast used in investigation

The mass changes were measured after 25, 50, 75, 100 and 150 h of exposure. The spalled oxide scale was not included in the weighing. Plan-view observations of the oxidized surfaces were made at various intervals during examination, via x-ray diffraction analysis (XRD) using X'Pert$^3$ Powder System, scanning electron microscopy (SEM) and energy-dispersive spectroscopy (EDS) using Hitachi S-3400N.

## 3. Results and Discussion

The cyclic oxidation performance of Co-Al-Mo-Nb and Co-Al-W Co-based superalloys at 800 °C is shown in Fig. 2. The considerably inferior oxidation resistance of Co-Al-Mo-Nb alloy compared to Co-Al-W alloy is observable. After first cycle, the mass of specimen corresponding to Co-Al-Mo-Nb slightly gained; however, each subsequent cycle resulted in decrease in the plot related to mass change of this alloy. In opposite to W-free alloy, the cyclic oxidation performance of Co-Al-W alloy was promising. The increasing trend of the plot related to Co-Al-W alloy implies that the oxide layer spallation occurred in considerably lower extent in comparison with that of Co-Al-Mo-Nb alloy.

The results of weight measurements during cyclic oxidation are reflected in the surface condition of oxidized specimens (Fig. 3). The external oxide layer of Co-Al-W alloy was gray and compact. This type of upper layer was retained to the end of examination; however, after 75, 100 and 150 h occurred some discolorations on the oxidized surface. Similar gray layer was observed in case of Co-Al-Mo-Nb alloy after 25 h of oxidation at 800 °C. Although the surface was relatively uniform, the single areas characterized by spallation of the external layer were observed and are indicated by black arrows in Fig. 3. The mass decrease after 50 h of oxidation was concomitant to the considerable amount of peeled oxides. The macrograph of specimen after second oxidation cycle reveals two characteristic types of scale, differing in color. The different scale types observed in the macrographs are marked by points (Fig. 3). The area marked by point no. 1 is corresponding to the same type of scale as observed after 25 h of oxidation. The surface of Co-Al-Mo-Nb alloy after 75 h of oxidation consists of three types of the oxide layer. The products of oxidation marked by point nos. 1–2 are oxides observed in the previous part of experiment. In this case, the oxide layer spallation and decrease in the specimen mass occurred as well. The outer layer of the specimen after 100 h of oxidation does not contain any new types of oxides. On the surface of alloy after last cycle of high-temperature exposure, the same types of oxides are observable in comparison with those of after 50 h of oxidation. Taking into account the color

**Table 1 Chemical composition of Co-Al-Mo-Nb and Co-Al-W as-cast alloys used in investigation**

| Nominal composition in at.% | Measured chemical composition in at.% | | | | |
|---|---|---|---|---|---|
| | Co | Al | W | Mo | Nb |
| Co-9Al-9W | 81.7 | 9.1 | 9.2 | … | … |
| Co-10Al-5Mo-2Nb | 84.8 | 4.63 | … | 4.6 | 2 |

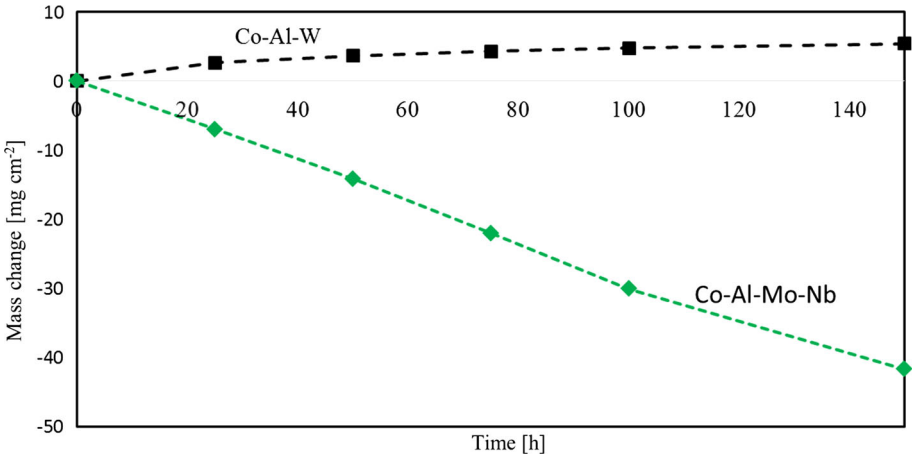


**Fig. 2** Cyclic oxidation of Co-Al-W and Co-Al-Mo-Nb Co-based superalloys at 800 °C

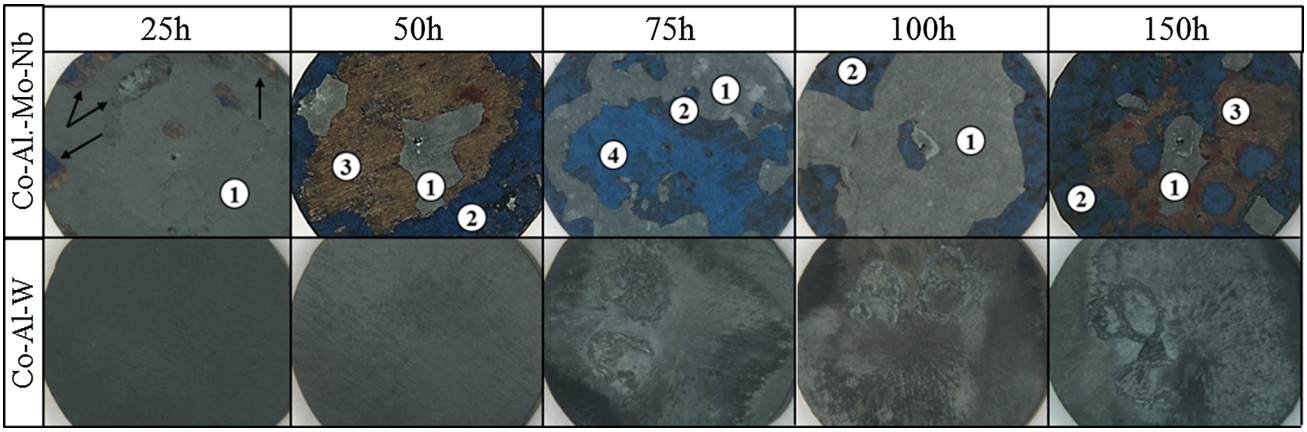


**Fig. 3** Macrographs of Co-Al-Mo-Nb and Co-Al-W Co-based superalloys' specimens after cyclic oxidation at 800 °C

contrast, four types of oxides were observed during entire experiment (Fig. 3).

High diversity of oxides present on the surface of Co-Al-Mo-Nb alloy after different cycles of high-temperature exposure implies that alternately occurring processes of scale growth and spallation had random character in opposite to that of Co-Al-W alloy, where the external layer was almost unchanging. The high variety of oxides present in the scale may exhibit negative influence on the layer adhesion, which was further observed in the experiment.

Figure 4 and 5 show the SEM imaging of oxidized surfaces after 25, 50, 75, 100 and 150 h of oxidation. Furthermore, the results of chemical composition analysis in microareas of the surface related to Fig. 4 and 5 are presented in Table 2, whereas the XRD patterns of oxidized surfaces are shown in Fig. 6. First cycle of oxidation resulted in the formation of the compact, gray external layer, which consists of tiny and irregular oxides, shown in Fig. 4. In view of the chemical composition, analyzed particles contain only Co and O. Furthermore, the XRD pattern of the surface after 25 h of oxidation (Fig. 6) shows the presence of $Co_3O_4$ (ICDD 42-1467) and CoO (ICDD 75-0533) as well. The appearance of $CoAl_2O_4$ (ICDD 44-0160) is possible as well due to quite similar XRD pattern compared to that of $Co_3O_4$, whereas taking into consideration the chemical composition and the literature data (Ref 13, 18), the presence of $Co_3O_4$ instead of $CoAl_2O_4$ is more reasonable. This type of oxide is predominant within the outer layer after 25 h of the high-temperature exposure.

The occurrence of three types of oxidized layer (Fig. 3-50 h) on the surface after 50 h of oxidation is confirmed in Fig. 4-50 h. The XRD pattern (Fig. 6-50 h) shows a complex phase composition of the oxidized surface, namely occurrence

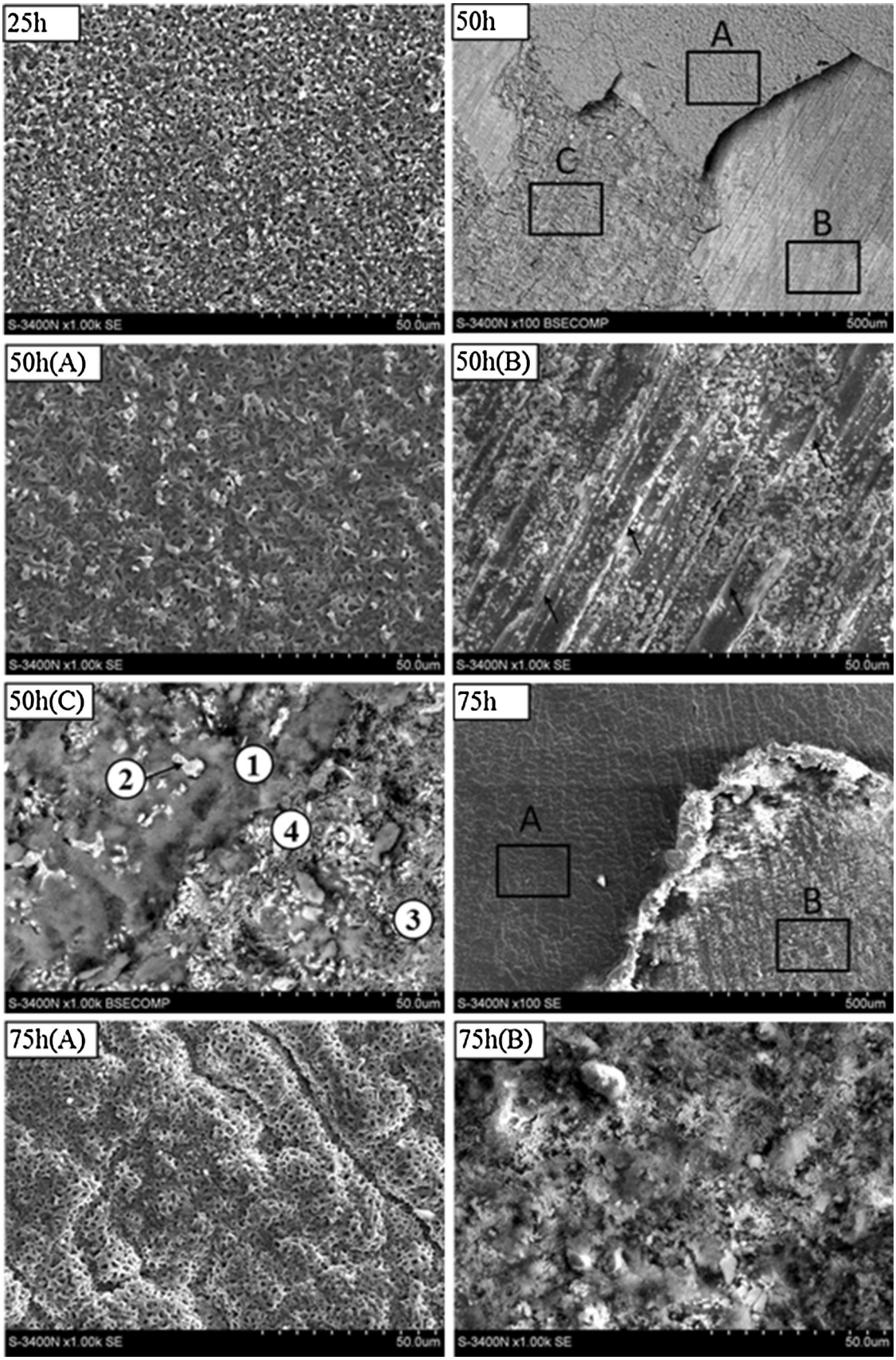


**Fig. 4** SEM images of Co-Al-Mo-Nb alloy after cyclic oxidation at 800 °C

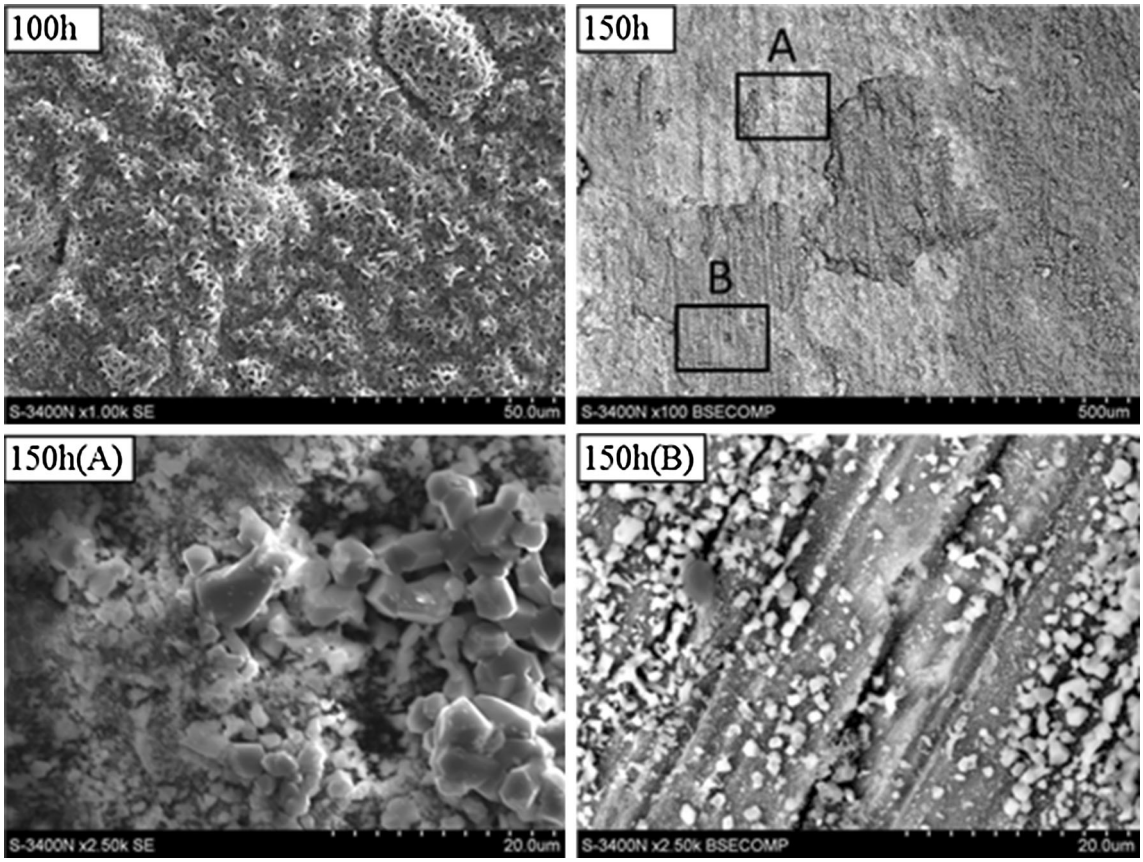


**Fig. 5** SEM images of Co-Al-Mo-Nb alloy after cyclic oxidation at 800 °C

**Table 2 Results of chemical composition analysis in areas and points marked in Fig. 4 and 5**

| | Element, at.% | | | | | Element, wt.% | | | | |
|---|---|---|---|---|---|---|---|---|---|---|
| **Area** | **Al** | **Co** | **Nb** | **Mo** | **O** | **Al** | **Co** | **Nb** | **Mo** | **O** |
| 25 h | | | | | | | | | | |
| Surface | … | 100 | … | … | + | … | 100 | … | … | + |
| 50 h | | | | | | | | | | |
| A | … | 100 | … | … | + | … | 100 | … | … | + |
| B | 14.7 | 78.7 | 5.7 | 0.9 | + | 7 | 82.1 | 9.3 | 1.6 | + |
| C | 28.2 | 55.4 | 7.5 | 8.8 | + | 13.7 | 58.6 | 12.6 | 15.2 | + |
| C(p.1) | 35.3 | 55.7 | 4.4 | 4.6 | + | 18.8 | 64.6 | 8 | 8.6 | + |
| C(p.2) | 21.1 | 44.4 | 34.5 | … | + | 8.9 | 41 | 50.1 | … | + |
| C(p.3) | 38 | 48.5 | 9.2 | 4.2 | + | 19.9 | 55.6 | 16.7 | 7.8 | + |
| C(p.4) | 23.5 | 49.5 | 4.6 | 22.4 | + | 10.4 | 47.6 | 6.9 | 35.1 | + |
| 75 h | | | | | | | | | | |
| A | 0.6 | 99.4 | … | … | + | 0.3 | 99.7 | … | … | + |
| B | 28.9 | 52.4 | 8.5 | 10.1 | + | 13.9 | 54.9 | 14 | 17.3 | + |
| 100 h | | | | | | | | | | |
| Surface | … | 100 | … | … | + | … | 100 | … | … | + |
| 150 h | | | | | | | | | | |
| A | 4.1 | 86.1 | … | 9.7 | + | 1.8 | 82.9 | … | 15.3 | + |
| B | 18.8 | 73.1 | 5 | 3.2 | + | 9.1 | 77.2 | 8.3 | 5.5 | + |

of $Co_3O_4$ (ICDD 42-1467), $CoNb_2O_6$ (ICDD 32-0304), $Co_2Mo_3O_8$ (ICDD 34-0511), CoO (ICDD 75-0533), $Co_2Nb_5O_{14}$ (ICDD 42-0422) and $Co_4Nb_2O_9$ (ICDD 38-1457) within investigated area. The presence of $CoAl_2O_4$ (ICDD 44-0160) is also possible due to great similarity of XRD pattern compared to that of $Co_3O_4$. The area marked with the letter A is morphologically similar to scale after 25 h of oxidation, whereas the size of oxide particles is increased compared to that of previous state. The chemical composition analysis revealed the presence of Co and O in this zone. The $Co_3O_4$ detected via x-ray diffraction analysis is presumably predominant phase present in this zone in analogy to surface condition after previous oxidation cycle. It is observable that exposure of other zones visible in Fig. 4-50 h is a result of spallation of the

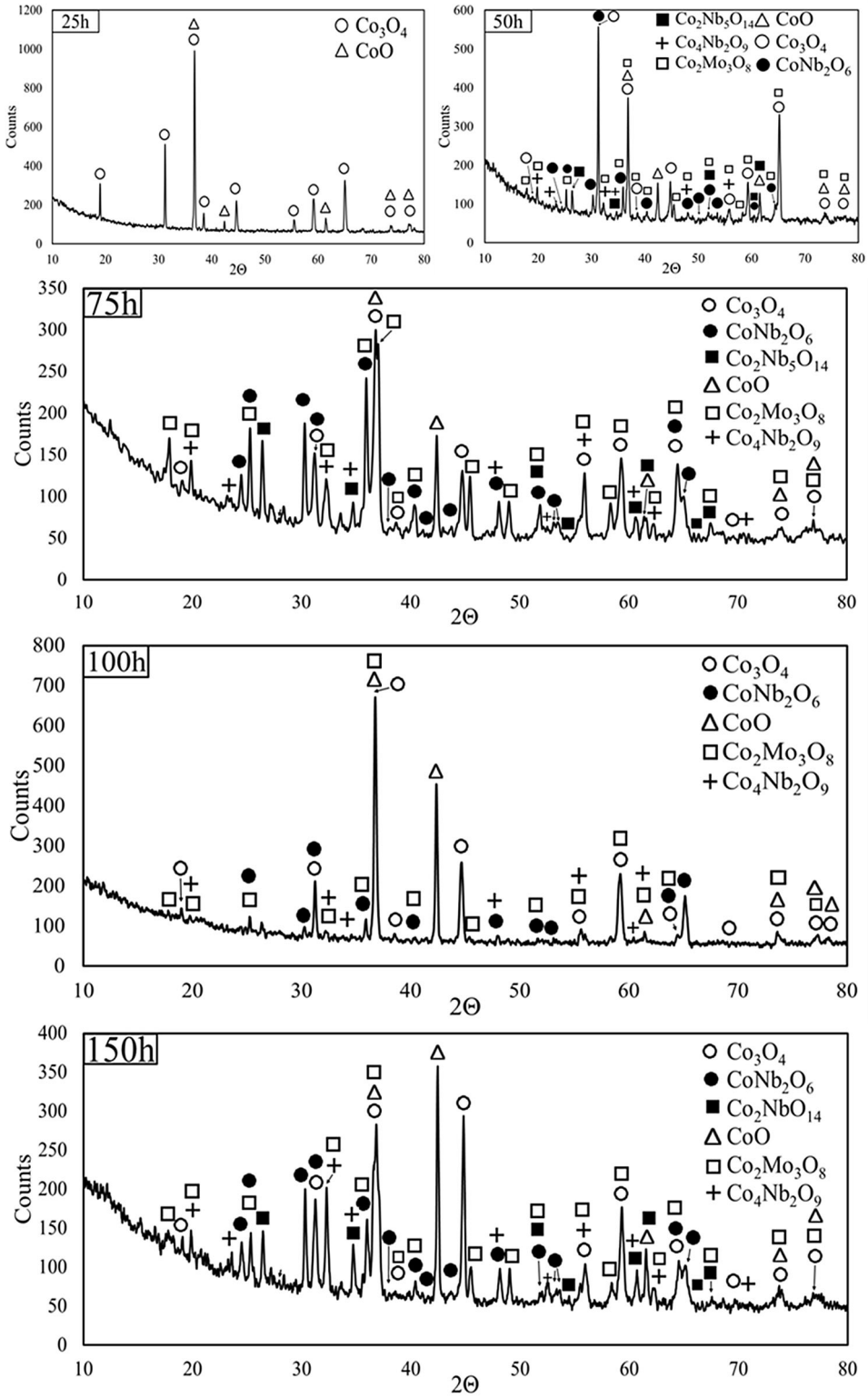


**Fig. 6** XRD patterns of Co-Al-Mo-Nb Co-based superalloy surface after cyclic oxidation at 800 °C

previously described layer related to decrease in specimen mass (Fig. 2). The another present zone marked with the letter B is related to area represented by point no. 3 in Fig. 3-50 h. This match is based on a ground topography of this area, visible in both Fig. 3-50 h and 4-50 h. The bands marked by black arrows are result of grinding in phase of specimen preparation. This fact leads to conclusion that in this area, the scale peeled out in a great extent and uncovered the substrate alloy. However, on the substrate alloy's surface, the small oxide particles are retained. The chemical composition measured in this zone shows the considerably increased content of Nb (9.3 at.%), compared to that of substrate alloy. This difference

may indicate that Nb-rich oxides detected via XRD analysis are present. The decreased amount of Mo in comparison with that of substrate alloy may be connected with diffusion of Mo and subsequent formation of volatile $MoO_3$ oxide. The last characteristic zone marked with the letter C may be associated with the area marked by point no. 2 in Fig. 2-50 h. It is observable that in areas free of spallation, this layer is covered by layer marked by the letter A. The light contrast shows the occurrence of few zones, different in chemical composition; thus, zone consists of more than one type of oxide. The oxidation products marked by point nos. 1 and 3 (Fig. 4-50 h(C)) are similar in view of chemical composition; however, higher content of Nb was measured in point no. 3. The small irregular oxide particles related to point no. 2 are considerably enriched in Nb, which may be related to the occurrence of Nb-rich oxides discussed earlier. Furthermore, the tiny oxidation products marked by point no. 4 are Mo-rich and may be recognized as the $Co_2Mo_3O_8$ oxide, detected via x-ray diffraction analysis.

The color contrast visible in Fig. 3-75 h indicated the presence of three types of oxidized layers; however, the SEM observations show occurrence of two different oxidized zones (Fig. 4-75 h). The diffraction peaks intensity present in the XRD pattern of surface after 75 h of oxidation is different compared to that of analogous XRD pattern after 50 h of exposure at 800 °C; however, the same six phases were detected within entire surface of specimen. The zone marked by the letter A (Fig. 4-75 h(A)) is comparable to zone after first oxidation cycle (Fig. 4-25 h) and zone after 50 h of high-temperature exposure (Fig. 4-50 h(A)) in view of chemical composition and morphology of oxide particles. Nevertheless, one difference was observed; namely, the oxides growth mechanism in this case resulted in a bumpy surface topography of the outer layer. The another present type of the external layer, analogous to that of area marked by point no. 2 in the macrograph (Fig. 3-75 h), is marked by the letter B (Fig. 4-75 h(B)). This zone may consist of various types of oxides and is similar to oxidized area after 50 h of high-temperature exposure (Fig. 4-50 h(C)) in view of chemical composition and morphology.

The external layer structure after 100 h of oxidation was dominated by gray, oxide layer type, marked by point no. 1 (Fig. 3-100 h), which was discussed in the analysis of previous oxidation cycles. The x-ray diffraction pattern (Fig. 6-100 h) showed the presence of the same phases compared to those of previous three cycles of oxidation, excluding $Co_2Nb_5O_{14}$. Furthermore, the great differences in the peaks intensity are observable. The XRD pattern implies that after 100 h of oxidation, the predominant phase within the scale is $Co_3O_4$, which is in great accordance with the surface fraction of previously discussed type of layer. The intensity of peaks related to oxides rich in Mo and Nb is decreased in comparison with that of previous x-ray diffraction pattern. The lower intensity of peaks may indicate decreased content of Mo- and Nb-rich oxides within the scale after 100 h of oxidation. The dominant type of external layer after 100 h of exposure at 800 °C is visible in microscale in Fig. 5-100 h. Taking into consideration the chemical composition and morphology, no substantial differences were observed between the discussed area and analogous zone of oxidized layer after 75 h of oxidation (Fig. 5-75 h(A)).

The last cycle of the high-temperature oxidation resulted in exposure of the areas marked by point nos. 2–3 (Fig. 3-150 h). The XRD pattern of scale after 150 h of oxidation (Fig. 6-

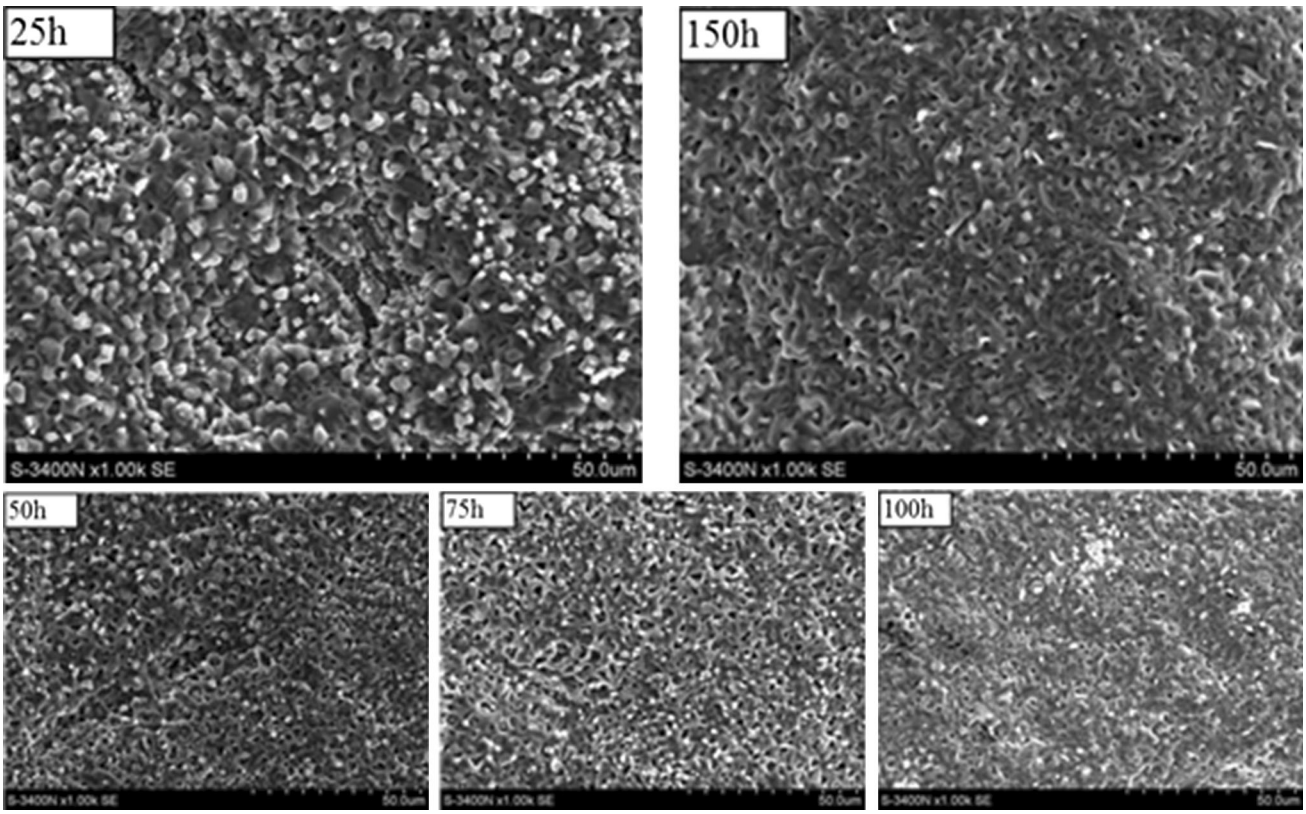


**Fig. 7** SEM images of Co-Al-W alloy after cyclic oxidation at 800 °C

**Table 3 Results of chemical composition analysis in areas and points marked in Fig. 7**

| Area | Element, at.% | | | | Element, wt.% | | | |
|---|---|---|---|---|---|---|---|---|
| | Al | Co | W | O | Al | Co | W | O |
| 25 h | | | | | | | | |
| Surface | 0.2 | 99.8 | … | + | 0.5 | 99.5 | … | + |
| 50 h | | | | | | | | |
| Surface | … | 100 | … | + | … | 100 | … | + |
| 75 h | | | | | | | | |
| Surface | … | 100 | … | + | … | 100 | … | + |
| 100 h | | | | | | | | |
| Surface | … | 100 | … | + | … | 100 | … | + |
| 150 h | | | | | | | | |
| Surface | 0.2 | 99.8 | … | + | 0.5 | 99.5 | … | + |

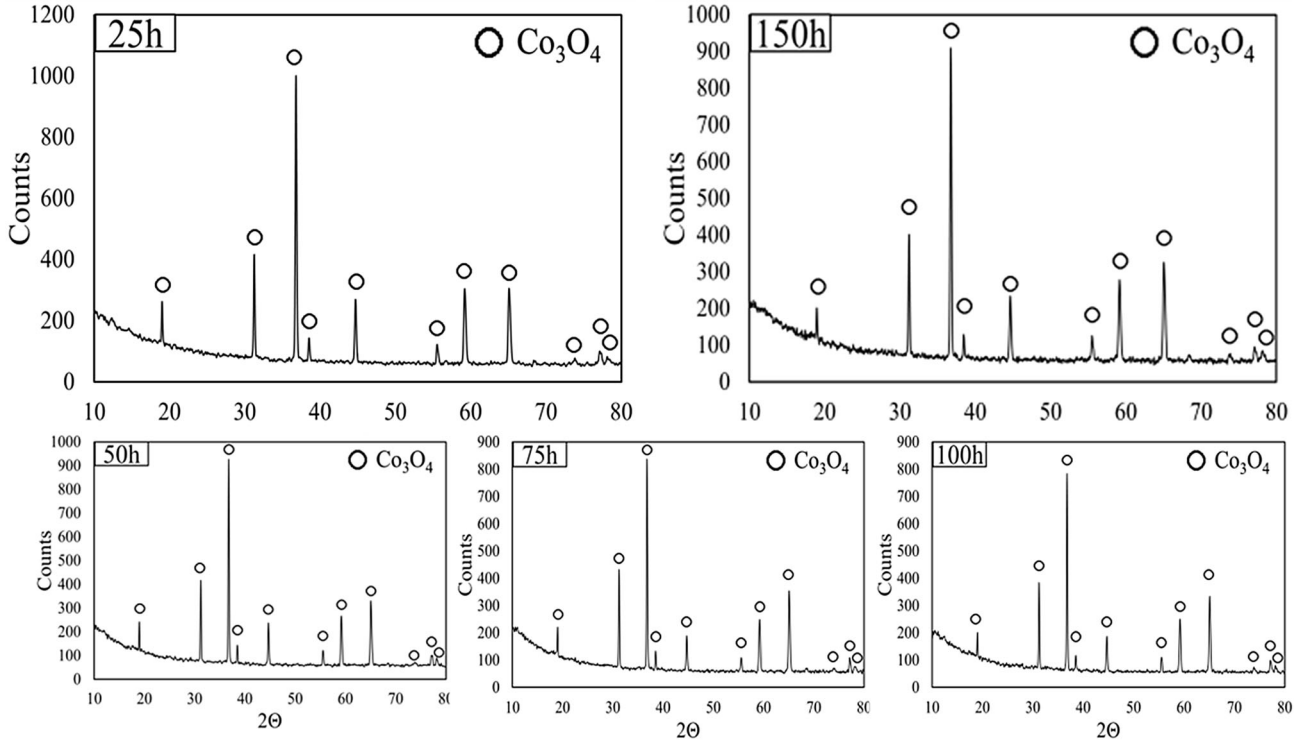


**Fig. 8** XRD patterns of Co-Al-Mo-W Co-based superalloy surface after cyclic oxidation at 800 °C

150 h) shows increased content of oxides rich in Mo and Nb, related to scale after 100 h of high-temperature exposure. In comparison with the surface condition after 50 and 75 h of oxidation, the same phases were detected after fourth cycle of the high-temperature exposure. The SEM micrograph of the oxidized surface shows two characteristic zones; one of them was not observed earlier. This new zone marked by the letter A consists of the oxide crystals of various sizes (Fig. 5-150 h(A)). The chemical composition analysis in this area showed the dominant content of Co, around twice higher amount of Mo compared to that of substrate alloy and lack of Nb. The content of Al in the investigated area was roughly 4 at.%. The chemical composition in this area may be related to the occurrence of oxides rich in Co and Mo. The second observed characteristic area marked by the letter B is shown in Fig. 5-150 h(B). Both morphologies of the surface and chemical composition indicate that the discussed outer layer is in great extent similar to analogous layer (Fig. 4-50 h(B)), which was discussed particularly.

Afterward, the surface condition after oxidation of the reference Co-9Al-9W (at.%) alloy was evaluated. Figure 7 shows SEM imaging of the oxidized surfaces after 25, 50, 75, 100 and 150 h of oxidation. Furthermore, the results of chemical composition analysis in microareas of the surface related to Fig. 7 are presented in Table 3, whereas the XRD patterns of the oxidized surfaces are shown in Fig. 8. The porous oxidized layer formed after 25 h of oxidation is composed of microparticles of oxides rich in Co. Investigated area is uniform in view of phase composition. The only detected phase was $Co_3O_4$ (ICDD 42-1467); however, existence of $CoAl_2O_4$ (ICDD 44-0160) is also possible since similarity of its XRD pattern compared to $Co_3O_4$ is substantial.

Taking into account the morphology, chemical and phase composition of the external layer, no substantial changes were observed after further cycles of the high-temperature exposure. The surface condition continuity during entire experiment is in great accordance with the macroscopic observations (Fig. 3). Taking into consideration the comparison of stable surface condition of Co-Al-W alloy and variable condition of scale in W-free alloy, the cause of considerable cyclic oxidation disparities between the investigated alloys is explicable. Furthermore, the scale grown after high-temperature oxidation of Co-Al-W alloy is uniform in view of phase composition; thus, less value of stress may be generated within scale during cooling. In contrast, the scale grown on substrate of the Co-Al-Mo-Nb is characterized by complex phase composition. The spallation of oxidized layer during cooling may be associated with variety of phases, hence variety of thermal expansion coefficient, being potential cause of oxide layer peeling. Furthermore, the stability of oxides present within the scale plays an important role in adhesion of the external layer. In case of pure Co, above 700 °C coexist two stable oxides (CoO and $Co_3O_4$). Furthermore, with increasing temperature, the CoO phase grows at the expense of $Co_3O_4$ up to 900 °C, wherefore at higher temperature only CoO is thermodynamically stable. Below 700 °C, the $Co_3O_4$ is predominant oxide in the scale grown on the pure Co and Co-based alloys (Ref 29, 30). In case of alloys, the alloying elements react with oxygen as well, resulting in the formation of other types of oxides. For Ni-Mo alloys and conventional Co-Mo alloys, the oxidation at 800 °C results in the formation of, respectively, NiO, $MoO_3$, $NiMoO_4$ and $Co_3O_4$, CoO, $MoO_3$, $CoMoO_4$ oxides (Ref 31, 32). The $MoO_3$ volatilizes above 700 °C, a part of volatile oxides deposit on the cooler section of the furnace, whereas rest may react with the other oxides or basic alloy in gas form (Ref 33). In case of the Ni-Mo alloys, Mo can oxidize to $MoO_2$ and $MoO_3$ and then subsequently reacts with Ni to form $NiMoO_4$ (Ref 6). The $NiMoO_4$ has been known to exhibit approximately 20% of volume change upon cooling due to the transformation of β to α phase at 250 °C (Ref 34, 35). This type of transition may occur also in case of Co-Mo-O system, namely during cooling of $CoMoO_4$ oxide (Ref 36, 37). The massive volume changes may increase spallation of the scale in Co-Al-Mo-Nb alloys. The two stable phases existing in the ternary system Co-Mo-O are $Co_2Mo_3O_8$ and $CoMoO_4$ (Ref 38); the second one was not detected in the present study. The formation of NbO, $NbO_2$ and $Nb_2O_5$ is expected during oxidation of pure Nb; however, in the temperature range 700-900 °C in the Co-Mo-Nb-O system, Co-oxides react with $Nb_2O_5$ resulting in the formation of cobalt molybdates ($CoNb_2O_6$ and $Co_4Nb_2O_9$) (Ref 39, 40). The $CoNb_2O_6$ exhibits two crystal structures: rutile and columbite, which considerably differ in lattice parameters (Ref 41). Despite spallation of oxides, the W-free alloys exhibit considerably higher oxidation rate. According to the literature data, the substitution of W by Mo and Nb may cause considerable deterioration of oxidation resistance mainly due to the formation of $MoO_3$ oxide, which starts volatilizing around 700 °C as $(MoO_3)_3$. $(WO_3)_3$ on the other hand will volatilize at higher temperatures (above 1300 °C) (Ref 33). Furthermore, another deleterious factor is the formation of highly porous $Nb_2O_5$ oxide, which adheres to the surface, provides a continuous patch for oxygen and subsequently allows formation of the mixed oxides. Furthermore, this oxide tends to react with base element and form cobalt molybdates, which may change the crystal structures upon temperature changes.

## 4. Conclusions

- The examination of the oxidation performance of Co-Al-Mo-Nb and Co-Al-W Co-based superalloys in as-cast state at 800 °C was performed. The considerably inferior oxidation behavior of Co-Al-Mo-Nb alloy compared to that of Co-Al-W alloy is observable. In case of W-free alloy, the specimen mass decrease, related to the oxide layer spallation, was observed repeatedly, while for Co-Al-W alloy the steady growth of scale was observed.
- The surface condition after each cycle of the exposure at 800 °C in air environment was determined in detail. Four characteristic types of the external layer were observed. Most of the oxidized layers were characterized by the complex phase structure, including the oxides rich in Co, Nb and Mo. The high phase diversity within the scale is unfavorable and may be the cause of low oxidation resistance under applied conditions. Various phases are characterized by different thermal expansion coefficients; therefore, stresses are generated during high-temperature intervals, resulting in the oxide layer spallation. Moreover, the phase stability of formed oxides and compounds, including cobalt molybdates and niobates, plays the important role in oxidation behavior of investigated alloy. The scale grown on Co-Al-W alloy's substrate was characterized as well. In this case, the external layer was uniform in view of morphology, chemical and phase composition. No substantial changes were observed during experiment, which is in good accordance with weight measurements.
- The substitution of W with Mo and Nb caused deterioration of the oxidation resistance at 800 °C. It is necessary to examine other elements promoting formation of $\gamma'$ phase, characterized by lower density compared to that of W, as a potential W-replacement for heat-resistant alloys exposed to high-temperature oxidation. New W-free Co-10Al-5Mo-2Nb (at.%) Co-based superalloy in as-cast state is not acceptable for high-temperature applications due to the insufficient high-temperature oxidation resistance.

### Acknowledgments

This work was supported by Institute of Materials Engineering of Silesian University of Technology, as a part of Statutory Research No. BK-225/RM3/2017.

## References


1. C.T. Sims, N.S. Stoloff, and W.C. Hagel, *Superalloys II*, Wiley, New York, 1987, p 135–163
2. T.M. Pollock and S. Tin, Nickel-Based Superalloys for Advanced Turbine Engines: Chemistry, Microstructure, and Properties, *Journal of Propulsion and Power*, 2006, **22**, p 361–374
3. S.K. Makineni, B. Nithin, and K. Chattopadhyay, Synthesis of a New Tungsten-Free γ–γ′ Cobalt-Based Superalloy by Tuning Alloying Additions, *Acta Materialia*, 2015, **85**, p 85–94
4. A.P. Bond and H.H. Uhlig, Corrosion Behavior and Passivity of Nickel–Chromium and Cobalt–Chromium Alloys, *Journal of Electrochemical Society*, 1960, **107**, p 488–493
5. A. Kocijan, I. Milosev, and B. Pihlar, Cobalt-Based Alloys for Orthopaedic Applications Studied by Electrochemical and XPS Analysis, *Journal of Materials Science: Materials in Medicine*, 2004, **15**, p 634–650
6. C. Montero-Ocampo and J.A. Hidalgo Badillo, EIS Study of the Electrochemical Behavior of the Co-Cr-Mo Alloy in Borate Solutions, *Electrochemical Society*, 2008, **11**, p 69–78
7. D. Mareci, D. Sutiman, A. Cailean, and G. Bolat, Comparative Corrosion Study of Ag-Pd and Co-Cr Alloys Used in Dental Applications, *Bulletin of Materials Science*, 2010, **33**, p 491–500
8. J. Sato, T. Omori, K. Oikawa, I. Ohnuma, R. Kainuma, and K. Ishida, Cobalt-Base High-Temperature Alloys, *Science*, 2006, **312**, p 90–91
9. T.M. Pollock, J. Dibbern, M. Tsunekane, J. Zhu, and A. Suzuki, New Co-Based γ–γ′ High Temperature Alloys, *The Journal of The Minerals, Metals and Materials Society*, 2010, **62**, p 58–63
10. A. Suzuki, G.C. Denolf, and T.M. Pollock, Flow Stress Anomalies in γ/γ′ Two-Phase Co-Al-W-Base Alloys, *Scripta Materialia*, 2007, **56**, p 385–388
11. A. Suzuki and T.M. Pollock, High-Temperature Strength and Deformation of γ/γ′ Two-Phase Co-Al-W-Base Alloys, *Acta Materialia*, 2008, **56**, p 1288–1297
12. L. Klein, Y. Shen, M.S. Killian, and S. Virtanen, Effect of B and Cr on the High Temperature Oxidation Behaviour of Novel γ/γ′-Strengthened Co-Base Superalloys, *Corrosion Science*, 2011, **53**, p 2713–2720
13. L. Klein, A. Bauer, S. Neumeier, M. Goken, and S. Virtanen, High Temperature Oxidation of γ/γ′-Strengthened Co-Base Superalloys, *Corrosion Science*, 2011, **53**, p 2027–2034
14. L. Klein and S. Virtanen, Corrosion Properties of novel γ′-Strengthened Co-Base Superalloys, *Corrosion Science*, 2013, **66**, p 233–241
15. L. Klein and S. Virtanen, Electrochemical Characterisation of Novel γ/γ′-Strengthened Co-Base Superalloys, *Electrochimica Acta*, 2012, **76**, p 275–281
16. G. Moskal, D. Migas, A. Tomaszewska, T. Mikuszewski, T. Maciąg, M. Godzierz, and D. Niemiec, Oxidation Performance of Co-Al-W and Co-Ni-Al-W New Type γ–γ′ Cobalt-Based Superalloys, *Materials Engineering*, 2017, **4**, p 163–169
17. H.-Y. Yan, V.A. Vorontsov, and D. Dye, Alloying Effects in Polycrystalline γ′ Strengthened Co-Al-W Base Alloys, *Intermetallics*, 2014, **48**, p 44–53
18. H.-Y. Yan, V.A. Vorontsov, J. Coakley, N.G. Jones, H.J. Stone, and D. Dye, Quaternary Alloying Effects and the Prospects for a New Generation of Co-Base Superalloys, in *Superalloys 2012: 12th International Symposium on Superalloys*, 2012, p 705–714
19. H.-Y. Yan, V.A. Vorontsov, and D. Dye, Effect of Alloying on the Oxidation Behaviour of Co-Al-W Superalloys, *Corrosion Science*, 2014, **83**, p 382–395
20. J.R. Davis, Ed., *Heat Resistant Materials*, 1st ed., ASM International, Novelty, 1997
21. A. Suzuki, H. Inui, and T.M. Pollock, $L1_2$-Strengthened Cobalt-Base Superalloys, *Annual Review of Materials Research*, 2015, **45**, p 345–368
22. F. Xue, Z.Q. Li, and Q. Feng, Mo Effect on the Microstructure in Co-Al-W-Based Superalloys, in *Materials Science Forum*, vol. 654–656, 2010, p 420–423
23. Q. Yao, S.-L. Shang, Y.-J. Hu, Y. Wang, Y. Wang, Y.H. Zhu, and Z.-K. Liu, First-Principles Investigation of Phase Stability, Elastic and Thermodynamic Properties in L12 Co3(Al, Mo, Nb) Phase, *Intermetallics*, 2016, **78**, p 1–7
24. S.K. Makineni, B. Nithin, D. Palanisamy, and K. Chattopadhyay, Phase Evolution and Crystallography of Precipitates During Decomposition of New "Tungsten-Free" Co(Ni)-Mo-Al-Nb γ/γ′ Superalloys at Elevated Temperatures, *Journal of Materials Science*, 2016, **51**, p 7843–7860
25. S.K. Makineni, A. Samanta, T. Rojhirunsakool, T. Alam, B. Nithin, A.K. Singh, R. Banerjee, and K. Chattopadhyay, A New Class of High Strength High Temperature Cobalt Based γ–γ′ Co–Mo–Al Alloys Stabilized with Ta Addition, *Acta Materialia*, 2015, **97**, p 29–40
26. S.K. Makineni, B. Nithin, and K. Chattopadhyay, A New Tungsten-Free γ–γ′ Co-Al-Mo-Nb-Based Superalloy, *Scripta Materialia*, 2014, **98**, p 36–39
27. G. Moskal, D. Migas, D. Niemiec, and M. Godzierz, Oxidation Behavior of Co-Al-Mo-Nb and Co-Ni-Al-Mo-Nb New Tungsten-Free γ–γ′ Cobalt-Based Superalloys, *Corrosion Protection*, 2017, **60**, p 318–322
28. T. Mikuszewski, A. Tomaszewska, G. Moskal, D. Migas, and D. Niemiec, Primary Microstructure Characterization of New Type γ–γ′ Co-Al-W Cobalt-Based Superalloys, *Materials Engineering*, 2017, **2017**(5), p 217–223
29. N.N. Greenwood and A. Earnshaw, *Chemistry of the Elements*, 2nd ed., Butterworth-Heinemann, Oxford, 1997
30. A.J. Ellet, *Oxidation Permeation and Thermo-Chemical Stabillity of Oxygen Separation Membrane Materials for the Oxyfuel Process*, Rhenisch-Westfälische Technische Hohschile, Aachen, 2009
31. A. Ul-Hamid, H.M. Tawancy, A.I. Mohammed, S.S. Al-Jaroudi, and N.M. Abbas, Cyclic oxidation behaviour of a Ni-Mo-Cr alloy at 800 °C, *Anti-Corrosion Methods and Materials*, 2004, **51**, p 339–347
32. Y.-D. Zhang, Z.-G. Yang, C. Zhang, and H. Lan, Oxidation Behavior of Tribaloy T-800 Alloy at 800 and 1000 °C, *Oxidation of Metals*, 2008, **70**(3–4), p 229–239
33. T. Karahana, G. Ouyang, P.K. Ray, M.J. Kramer, and M. Akinc, Oxidation Mechanism of W Substituted Mo-Si-B Alloys, *Intermetallics*, 2017, **2017**(87), p 38–44
34. P.K. Ray, M. Akinc, and M.J. Kramer, Formation of Multilayered Scale During the Oxidation of NiAl-Mo Alloy, *Applied Surface Science*, 2014, **301**, p 107–111
35. J.L. Smialek, A. Garg, T.P. Gabb, and R.A. MacKay, Cyclic Oxidation of High Mo, *Reduced Density Superalloys, Metals*, 2015, **5**, p 2165–2185
36. K.T. Jacoba and S. Vana, Varamba: Phase Equilibria and Thermodynamic Properties of Ternary Oxides in the System Co-Mo-O, *Journal of Alloys and Compounds*, 1988, **280**, p 138–146
37. H. Ehrenberg, M. Knapp, and H. Weitzel, *Phase transitions and thermal expansion of polymorphic CoMoO4*. Institute for Materials Science, Darmstadt University of Technology Petersenstr. 23, 64287 Darmstadt
38. G.A. Rossetti, J.L. Burger, and R.D. Sisson, Characterization of Mixed Cobalt–Molybdenum Oxides Prepared by Evaporative Decomposition of Solutions, *Journal of the American Ceramic Society*, 1989, **72**, p 1811–1815
39. F. Gesmundo, Y. Niu, F. Viani, and F.C. Rizzo, An Analysis of the Internal Oxidation of Binary M-Nb Alloys Under Low Oxygen Pressures at 600-800 °C, *Oxidation of Metals*, 1996, **46**, p 441–463
40. A.G. Belous, O.V. Ovchar, A.V. Kramarenko, D.O. Mishchuk, B. Jancar, J. Bezjak, and D. Suvorov, Effect of Nonstoichiometry on the Structure and Microwave Dielectric Properties of Cobalt Metaniobate, *Inorganic Materials*, 2006, **42**, p 1369–1373
41. R. Ma, F. Cao, J. Wang, G. Zhu, and G. Pang, Hydrothermal Synthesis and Phase Stability of CoNb2O6 with a Rutile Structure, *Materials Letters*, 2011, **65**, p 2880–2882